J. Fluid Mech. (2012), *vol.* 705, *pp.* 149–164. © Cambridge University Press 2011
doi:10.1017/jfm.2011.506

Flapping propulsion using a fin ray

S. Alben†

School of Mathematics, Georgia Institute of Technology, Atlanta, GA 30332, USA

(Received 3 May 2011; revised 28 October 2011; accepted 15 November 2011;
first published online 21 December 2011)

We calculate optimal driving motions for a fin ray in a two-dimensional inviscid fluid, which is a model for caudal fin locomotion. The driving is sinusoidal in time, and consists of heaving, pitching and a less-studied motion called 'shifting'. The optimal phases of shifting relative to heaving and pitching for maximum thrust power and efficiency are calculated. The optimal phases undergo jumps at resonant combinations of fin ray bending and shear moduli, and are nearly constant in regions between resonances. In two examples, pitching- and heaving-based motions converge with the addition of optimal shifting. Shifting provides an order-one increase in output power and efficiency.

Key words: swimming/flying

1. Introduction

Recently, many studies have considered the hydrodynamic performances of flexible flapping foils, which are models for the bodies or fins of swimming fish (Prempraneerach, Hover & Triantafyllou 2003; Lauder *et al.* 2007; Lauder & Madden 2007; Akhtar *et al.* 2007; Michelin & Smith 2009; Miller & Peskin 2009; Shelley & Zhang 2011). In this work, we study the hydrodynamic performance of a flexible foil which includes the internal mechanics of fish fins. Indeed, the supporting structures of flexible fish fins, called fin rays, contain an internal collagen network which allows for more shape control than is possible with a simple flexible foil (Videler 1993; Alben, Madden & Lauder 2007). The fin ray presents a relatively unexplored mechanism for enhanced propulsion, and is currently being used in biomimetic foils, so understanding its hydrodynamic performance is useful (Lauder *et al.* 2007; Tangorra *et al.* 2007; Zhu & Shoele 2008).

In our previous work (Alben *et al.* 2007), we derived a model for the mechanics of the fin ray, and now we briefly describe the main elements of the anatomy and mechanics. The fin ray can be considered as a pair of flexible rods, tied together with collagenous fibres (Videler 1993; Alben *et al.* 2007). The fish muscles have two or three attachments to each of the two rods in a typical fin ray, which allow for multiple motions within and out of the plane of the fin. Focusing only on the motions of the fin ray perpendicular to the plane of the fin, for simplicity, we obtain a model in which a one-dimensional rod-like object, with the mechanical structure of the fin ray, moves in a two-dimensional fluid. The collagenous fibres are the connecting elements for the bony segments in each of the two rods and are responsible

† Email address for correspondence: alben@math.gatech.edu

https://doi.org/10.1017/jfm.2011.506 Published online by Cambridge University Press

for the rods' flexibility. Additional collagenous fibres connect one rod to the other, running transversely through the thin layer of fluid which is sandwiched between them. When one of the rods is displaced (or 'shifted') axially relative to the other, these fibres are stretched and their resistance to stretching leads to a shear modulus for the two-rod structure. In Alben *et al.* (2007) we derived a beam-like equation for large deflections of the fin ray under shifting motions. We compared with experiments on actual specimens and found good agreement under different static loading conditions. In general, curvature is concentrated near where the shift is applied, at the base of the fin ray.

The ray-finned fishes include about half of all fish species and are the most derived fishes (Lauder 1989). Fin rays occur in most of the fins used for swimming, including the pectoral, dorsal, anal, pelvic and caudal fins (Videler 1993). Here we consider a fin ray in a two-dimensional cross-section of an oncoming flow past a caudal (tail) fin. The caudal fin is often the largest fin and the most important for generating thrust, particularly at higher swimming speeds. Our model can be considered a step towards incorporating more fully the internal mechanics of fish in propulsion studies (Cheng, Pedley & Altringham 1998; Pedley & Hill 1999).

2. Model

Our model uses the linear theory for small deflections of a flexible foil in a two-dimensional inviscid fluid. Although the theory assumes small deflections, it is also a reasonable approximation at the moderate deflections typical of a real caudal fin. We extend the model of Alben (2008), in which a passive elastic beam is driven by sinusoidal pitching at the leading edge. Here we consider instead a model fin ray, a bilaminate structure with internal resistance to shearing. The fin ray is driven by a combination of three motions – pitching, heaving and shifting – at the leading edge.

Figure 1 shows a schematic of a fin ray during each of the three motions separately. In each case, the fin ray encounters a flow with velocity V_x directed at its leading edge. Here V_x takes on a prescribed value; the fin ray does not swim freely. Rather, like previous works on flexible foils (Katz & Weihs 1978; Alben 2008), we consider the fin ray to be analogous to a ship propeller: the fin ray produces a thrust force which may be used to overcome the drag force on the rest of the fish body. The thrust force corresponds to the rate at which momentum is added to the fluid stream. Subsequently in this paper, we determine driving motions which maximize the thrust force on the fin ray, for realistic values of V_x. In figure 1(a), the fin ray is shown at two instants during a periodic heaving motion: at the peak and trough of heaving displacement at the leading edge. The fin ray is drawn as two nearly parallel curved lines with 20 much shorter straight line segments connecting them. The two curved lines represent the bilaminate structure of the fin ray, and each curved line consists of bony segments connected by collagenous fibres (Videler 1993). The 20 shorter line segments represent additional collagenous fibres which connect the two lines. Each curved line is modelled by a beam with uniform bending modulus B. The region between the beams is modelled as a linearly elastic material with uniform shear modulus per unit length G. Shearing the region between the beams stretches the collagenous fibres running between them, which results in a shear modulus. This model allows us to explore how a fin ray interacts with a flow using just two elastic parameters, B and G. Our previous work (Alben *et al.* 2007) explains in more detail how B and G arise from the fin ray structure, and Alben *et al.* (2007) and Alben & McGee (2010) have considered non-uniform B and G.

https://doi.org/10.1017/jfm.2011.506 Published online by Cambridge University Press

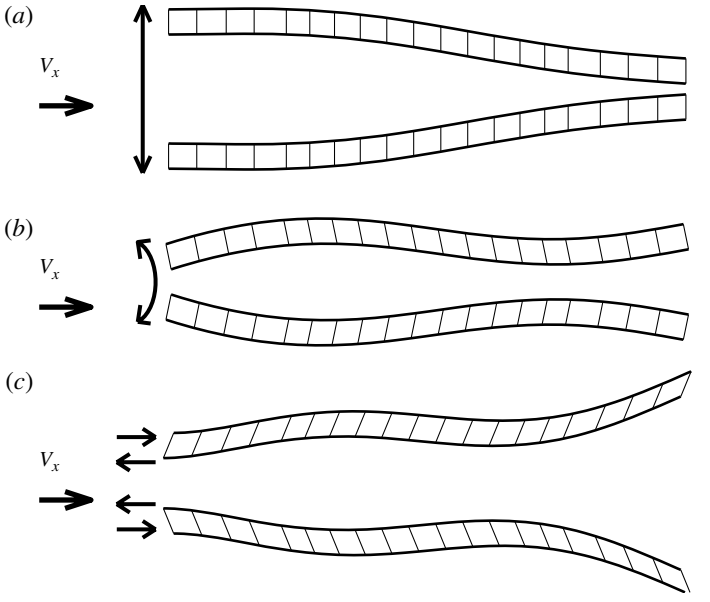


FIGURE 1. Schematic diagrams of the fin ray motion during three types of leading edge driving: (*a*) heaving; (*b*) pitching; (*c*) shifting.

In figure 1(*a*), the fin ray flexes as it moves. Here the fin ray is considered in isolation from the tail fin. A real tail fin can be considered a thin fin-ray-stiffened plate. The plate is a composite structure consisting of 10–15 nearly parallel rod-like elements, the fin rays, which are sheathed in a stretchable skin membrane. Imagining the tail fin as a wing in a three-dimensional flow, we take a two-dimensional cross-section through the flow and the chord of the tail fin, at a fixed spanwise location. We thus approximate the tail fin as a one-dimensional rod with the mechanical properties of a single fin ray, immersed in two-dimensional flow field. The two-dimensional fluid density can be set to the three-dimensional fluid density times the width of the layer of fluid which interacts with a single fin ray. This width is the same as the spacing between the fin rays in the spanwise direction along the fin.

Figure 1(*b*) is the same as figure 1(*a*) except that the fin ray is now being pitched at the leading edge. The instants of maximum and minimum pitch angle are shown. The fin ray flexes differently from figure 1(*a*) and the collagenous fibres are now non-vertical, although this is simply an artifact of the drawing: the fibres could easily be non-vertical in the heaving case (figure 1*a*) as well. In figure 1(*c*), we sketch the fin ray during a shifting motion. This motion is relatively new in the field of flexible flapping foils, unlike pitching and heaving. Here the arrows at the leading edge of the fin ray show a differential motion among the two halves of the fin ray, tangential shifting, which induces shear strain in the collagen fibres. This strain is partly relieved when the fin ray flexes, so shifting can alter the bending of the fin ray. As in figure 1(*a,b*), the shifting motion is shown at the peak and trough of amplitude. In figure 1(*c*) the fin rays at the two instants are displaced vertically only so they do not overlap: no heaving motion is implied.

The fin ray shapes in figure 1(*a,b,c*) result from a balance of bending forces in the two rods, shear forces in the layer of collagen between them and hydrodynamic forces on the outer surfaces of the fin rays. We now derive this force balance in the linearized case.

https://doi.org/10.1017/jfm.2011.506 Published online by Cambridge University Press

We assume that the heaving, pitching and shifting motions are sinusoidal in time, with a single frequency. However, the relative phases of the motions may be varied, and determining how to set these phases is a key aspect of this work.

We derive the equation for the fin ray deflection using Hamilton's principle applied to fluid–structure interactions (Paidoussis 1998):

$$\delta \int_{t_1}^{t_2} \mathscr{L}\, \mathrm{d}t + \int_{t_1}^{t_2} \delta W\, \mathrm{d}t, \tag{2.1}$$

where $\mathscr{L} = \mathscr{T} - \mathscr{V}$ is the Lagrangian, $\mathscr{T}$ and $\mathscr{V}$ being the kinetic and potential energies of the fin ray and δW the virtual work by fluid pressure forces on the fin ray. The kinetic energy for a fin ray with uniform mass per unit length ρ_s undergoing vertical deflections $y(x, t)$ about a flat state is

$$\mathscr{T} = \frac{1}{2}\rho_s \int_{-1}^{1} (\partial_t y(x, t))^2\, \mathrm{d}x, \tag{2.2}$$

and the potential energy, which is internal elastic energy, is

$$\mathscr{V} = \int_{-1}^{1} B(\partial_{xx} y(x, t))^2 + \frac{1}{2} G \left(\frac{\phi}{d}\right)^2 \mathrm{d}x. \tag{2.3}$$

Here ϕ is the tangential shift of the upper beam in the fin ray relative to the lower beam, and d is the distance separating them, which is also the thickness of the collagen layer. Thus, ϕ/d is the amount of shear in the collagen layer. An expression for ϕ was derived in terms of d and the local curvature of the fin ray in Alben *et al.* (2007). The small-deflection version is

$$\phi(x, t) = \phi(-1, t) - \int_{-1}^{x} d\, \partial_{xx} y(x, t)\, \mathrm{d}x. \tag{2.4}$$

Briefly, this equation can be understood by considering the two beams in the fin ray as curved lines which are constrained to be nearly parallel, by lubrication forces in the collagenous layer. When the fin ray becomes curved, both beams become curved, and this makes the beam closer to the centre of curvature shift tangentially forward relative to the other beam, by an amount given by (2.4). We now assume for simplicity that d is uniform, so

$$\phi(x, t) = \phi(-1, t) - d\left(\partial_x y(x, t) - \partial_x y(-1, t)\right). \tag{2.5}$$

Taking the variation of (2.3),

$$\delta \mathscr{V} = \int_{-1}^{1} (2B\partial_{xxxx} y(x, t) - G\partial_{xx} y(x, t))\, \delta y\, \mathrm{d}x \tag{2.6}$$

$$+ G\frac{\phi}{d^2}\delta\phi|_{-1} + G\frac{\phi}{d}\delta\partial_x y|_{-1} + 2B\partial_{xx} y \delta\partial_x y\,|_{-1}^{1} + \left(-2B\partial_{xxx} y - G\frac{\phi}{d}\right)\delta y\,|_{-1}^{1}. \tag{2.7}$$

The boundary terms in (2.7) are set by the conditions at the leading and trailing edge. At the leading edge, we assume sinusoidal driving in pitching, heaving and shifting,

$$y(-1, t) = \mathrm{Re}\left(A_0 \mathrm{e}^{\mathrm{i}2\pi t}\right); \quad \partial_x y(-1, t) = \mathrm{Re}\left(B_0 \mathrm{e}^{\mathrm{i}2\pi t}\right); \quad \phi(-1, t)/d = \mathrm{Re}\left(C_0 \mathrm{e}^{\mathrm{i}2\pi t}\right). \tag{2.8}$$

https://doi.org/10.1017/jfm.2011.506 Published online by Cambridge University Press

At the trailing edge, we assume free-end boundary conditions,

$$2B\partial_{xx}y(1,t)=0; \tag{2.9}$$

$$-2B\partial_{xxx}y(1,t)-G\left(\phi(-1,t)/d-\partial_x y(1,t)+\partial_x y(-1,t)\right)=0. \tag{2.10}$$

Taking the variation of the kinetic energy,

$$\delta\int_{t_1}^{t_2}\mathscr{T}\,\mathrm{d}t=\int_{t_1}^{t_2}\rho_s\int_{-1}^{1}\partial_{tt}y(x,t)\delta y\,\mathrm{d}x\,\mathrm{d}t. \tag{2.11}$$

The temporal boundary terms at t_1 and t_2 vanish if we assume periodic motion with t_1 and t_2 separated by a period.

The virtual work due to fluid pressure forces is

$$\int_{t_1}^{t_2}\delta W\,\mathrm{d}t=\int_{t_1}^{t_2}[p]\delta y\,\mathrm{d}t \tag{2.12}$$

where $[p]$ is the pressure jump across the fin ray. In appendix A we summarize the key results in the determination of $[p]$ and the inviscid flow around the fin ray; the details are given in Alben (2008).

Setting to zero the terms which multiply δy in (2.1), the equation of motion for the fin is

$$\rho_s\partial_{tt}y=-2B\partial_{xxxx}y+G\partial_{xx}y-[p]. \tag{2.13}$$

We have already non-dimensionalized lengths by the fin ray half-length L and time by the period of leading edge driving, T. We non-dimensionalize mass per unit area by the two-dimensional fluid density. We thus obtain a dimensionless form of (2.13) which we exclusively use from now on. We retain the same symbols for simplicity. When the ratio G/B is large, the curvature becomes concentrated near the leading edge (Alben *et al.* 2007). As explained in Alben (2008), the dimensionless ρ_s is $\sim 10^{-2}$ for a real fin ray, and may be set to zero without significantly affecting the results:

$$0=-2B\partial_{xxxx}y+G\partial_{xx}y-[p]. \tag{2.14}$$

We assume that the fin deflection, shift and pressure jump are sinusoidal in time:

$$y(x,t)=\mathrm{Re}\left(Y(x)\mathrm{e}^{2\pi\mathrm{i}t}\right);\ \phi(x,t)=\mathrm{Re}\left(\Phi(x)\mathrm{e}^{2\pi\mathrm{i}t}\right)\quad[p](x,t)=\mathrm{Re}\left(P(x)\mathrm{e}^{2\pi\mathrm{i}t}\right), \tag{2.15}$$

so (2.14) becomes an ordinary differential equation for complex-valued functions:

$$0=-2BY^{\mathrm{iv}}+GY''-P. \tag{2.16}$$

From (2.8) and (2.10), the boundary conditions are

$$Y(-1)=A_0;\quad Y'(-1)=B_0;\quad \Phi(-1)=C_0; \tag{2.17}$$

$$2BY''(1)=0;\quad -2BY'''(1)-G\left(C_0-Y'(1)+B_0\right)=0. \tag{2.18}$$

Because the equations are linear, we can decompose the solution into a linear combination of three solutions, each of which has unit amplitude in exactly one of the heaving, pitching and shifting motions, and zero in the other two. Thus, the 'pure heaving' solution (Y_{A1},Φ_{A1}) satisfies the boundary conditions

$$Y_{A1}(-1)=1;\quad Y'_{A1}(-1)=0;\quad \Phi_{A1}(-1)=0; \tag{2.19}$$

$$2BY''_{A1}(1)=0;\quad -2BY'''_{A1}(1)=0, \tag{2.20}$$

https://doi.org/10.1017/jfm.2011.506 Published online by Cambridge University Press

the 'pure pitching' solution (Y_{B1}, Φ_{B1}) satisfies the boundary conditions

$$Y_{B1}(-1) = 0; \quad Y'_{B1}(-1) = 1; \quad \Phi_{B1}(-1) = 0; \tag{2.21}$$

$$2BY''_{B1}(1) = 0; \quad -2BY'''_{B1}(1) - G\left(-Y'_{B1}(1) + 1\right) = 0, \tag{2.22}$$

and the 'pure shifting' solution (Y_{C1}, Φ_{C1}) satisfies the boundary conditions

$$Y_{C1}(-1) = 0; \quad Y'_{C1}(-1) = 0; \quad \Phi_{C1}(-1) = 1; \tag{2.23}$$

$$2BY''_{C1}(1) = 0; \quad -2BY'''_{C1}(1) - G\left(1 - Y'_{C1}(1)\right) = 0. \tag{2.24}$$

For each choice of the three control parameters (B, G, V_x), we obtain the general solution by superposing the three pure solutions scaled by A_0, B_0 and C_0:

$$Y_A = A_0 Y_{A1}; \quad Y_B = B_0 Y_{B1}; \quad Y_C = C_0 Y_{C1}; \quad Y = Y_A + Y_B + Y_C. \tag{2.25}$$

We give notation for the phases of the complex amplitudes:

$$A_0 = |A_0| e^{i\psi_A}; \quad B_0 = |B_0| e^{i\psi_B}; \quad C_0 = |C_0| e^{i\psi_C}. \tag{2.26}$$

The pure heaving and pure pitching solutions are similar to those presented in Alben (2008, 2009*c*), except that here (2.16) and boundary conditions (2.18) contain additional elastic terms proportional to G. The effect of G is to inhibit bending in these two solutions, because zero shift is imposed at the leading edge and curvature creates a non-zero shift through (2.4) and non-zero elastic shear energy in (2.3). However, in the pure shifting solution, bending is created by the shear elasticity G together with the shift imposed at the leading edge. Non-zero curvature occurs along the fin which decreases the shift in the fin ray through (2.4), and consequently decreases the elastic shear energy in (2.3).

As in previous works dealing with flexible flapping foils in a flow (Prempraneerach *et al.* 2003; Mittal 2004; Alben 2009*b*,*a*), we consider the optimization of two basic quantities: the output power and the efficiency. We focus on the shifting at the leading edge (C_0), which distinguishes this from previous flexible foil studies. We ask, in the three-parameter space (B, G, V_x), what phases of shifting relative to heaving $(\psi_C - \psi_A)$ and shifting relative to pitching $(\psi_C - \psi_B)$ maximize the output power and efficiency?

The output power is the product of V_x with the upstream force on the foil. Its period average is

$$\langle P_{out} \rangle = \int_0^1 \mathrm{d}t \int_{-1}^1 \mathrm{d}x \, (-V_x[p]\partial_x y) \tag{2.27}$$

$$= -\frac{1}{2} V_x \int_{-1}^1 \mathrm{Re}\left(P\overline{Y'}\right) \mathrm{d}x. \tag{2.28}$$

$$= -\frac{1}{2} V_x \int_{-1}^1 \mathrm{Re}\left((P_A + P_B + P_C)(\overline{Y'_A} + \overline{Y'_B} + \overline{Y'_C})\right) \mathrm{d}x. \tag{2.29}$$

We have neglected the thrust due to leading-edge suction, because the leading edge flow singularity is often unrealistic for flapping foils (Wang 2005; Eldredge, Toomey & Medina 2010; Alben *et al.* 2011). When the product in (2.29) is expanded, there are nine terms, which are quadratic in A_0, B_0, C_0. To simplify the results, we focus on the relative phases rather than the magnitudes of these complex amplitudes. It is easier to isolate the contribution of the relative phases under two assumptions which we now make. First, we assume that the driving motion is a combination of heaving and shifting only or pitching and shifting only. Thus, we can avoid choosing the

https://doi.org/10.1017/jfm.2011.506 Published online by Cambridge University Press

relative phase and magnitude of heaving and pitching, which simplifies our problem by eliminating some variables from consideration. Furthermore, the relation between heaving and pitching has been discussed in several previous works (Lighthill 1970; Wu 1971; Alben 2009*c*; Eldredge *et al.* 2010). The second assumption we make is that the amplitude of heaving or pitching is larger than that of shifting:

$$|A_0|^2, |B_0|^2 > |A_0||C_0|, |B_0||C_0| > |C_0|^2 . \tag{2.30}$$

The terms in (2.29) with amplitude proportional to the largest terms in (2.30) depend only on heaving and pitching, and not on shifting. The leading terms in (2.29) which depend on shifting correspond to the intermediate terms in (2.30), which are linear in shifting amplitude. These correspond to the interaction between heaving and shifting or pitching and shifting. These terms are our focus. We now identify the phase difference between heaving and shifting which maximizes the interaction term. We are maximizing

$$\langle P_{out,AC} \rangle \equiv -\frac{1}{2} V_x \int_{-1}^{1} \mathrm{Re}\left(P_A \overline{Y'_C} + P_C \overline{Y'_A}\right) \mathrm{d}x. \tag{2.31}$$

$$= -\frac{1}{2} V_x |A_0||C_0| \mathrm{Re}\left(\mathrm{e}^{\mathrm{i}(\psi_A - \psi_C)} \int_{-1}^{1} P_{A1} \overline{Y'_{C1}} + \overline{P_{C1}} Y'_{A1} \, \mathrm{d}x\right). \tag{2.32}$$

The phase difference which maximizes this contribution to the output power is

$$\psi_C - \psi_A = \mathrm{Arg}\left(-\int_{-1}^{1} P_{A1} \overline{Y'_{C1}} + \overline{P_{C1}} Y'_{A1} \, \mathrm{d}x\right). \tag{2.33}$$

In a motion with pitching and shifting only, the phase difference which maximizes the cross-term in the output power is

$$\psi_C - \psi_B = \mathrm{Arg}\left(-\int_{-1}^{1} P_{B1} \overline{Y'_{C1}} + \overline{P_{C1}} Y'_{B1} \, \mathrm{d}x\right). \tag{2.34}$$

We now consider the efficiency, which we define to be

$$\eta = \langle P_{out} \rangle - \langle P_{in} \rangle \tag{2.35}$$

with $\langle P_{out} \rangle$ given above and

$$\langle P_{in} \rangle = \int_0^1 \mathrm{d}t \int_{-1}^{1} \mathrm{d}x \, ([p] \partial_t y) \tag{2.36}$$

$$= \frac{1}{2} \int_{-1}^{1} \mathrm{Re}\left(P \overline{2\pi \mathrm{i} Y}\right) \mathrm{d}x. \tag{2.37}$$

$$= \frac{1}{2} \int_{-1}^{1} \mathrm{Re}\left(-2\pi \mathrm{i}(P_A + P_B + P_C)(\overline{Y_A} + \overline{Y_B} + \overline{Y_C})\right) \mathrm{d}x. \tag{2.38}$$

Other definitions of efficiency, such as the Froude efficiency ($\langle P_{out} \rangle / \langle P_{in} \rangle$), can also be used. Many works have considered the Froude efficiency, such as Lighthill (1970), Prempraneerach *et al.* (2003) and Mittal (2004), and there are alternative definitions of efficiency (Schultz 2002).

The disadvantage of using the Froude efficiency here is that the amplitude of shifting relative to the other two motions enters as an additional parameter. Under the same assumptions as in (2.30), we expand η to linear order in C_0, and select the phases which maximize the terms in η which are linear in C_0.

https://doi.org/10.1017/jfm.2011.506 Published online by Cambridge University Press

Following the same steps as above, the phase differences which maximize the linear contribution to the efficiency are

$$\psi_C - \psi_A = \mathrm{Arg}\left(\int_{-1}^{1}\left(P_{A1}\overline{\left(-V_x Y'_{C1} - 2\pi \mathrm{i} Y_{C1}\right)} + \overline{P_{C1}}\left(-V_x Y'_{A1} - 2\pi \mathrm{i} Y_{A1}\right)\right)\mathrm{d}x\right), \quad (2.39)$$

$$\psi_C - \psi_B = \mathrm{Arg}\left(\int_{-1}^{1}\left(P_{B1}\overline{\left(-V_x Y'_{C1} - 2\pi \mathrm{i} Y_{C1}\right)} + \overline{P_{C1}}\left(-V_x Y'_{B1} - 2\pi \mathrm{i} Y_{B1}\right)\right)\mathrm{d}x\right). \quad (2.40)$$

The power- and efficiency-maximizing phase differences (2.33), (2.34), (2.39) and (2.40) are functions of (B, G, V_x). We present results for a range of realistic values of B and G, at two values of V_x which correspond to realistic swimming speeds.

3. Results

In figure 2, we give greyscale maps of the optimal shifting phases at $V_x = \pi/3$. For clarity, we use only four different shadings. White corresponds to phase differences in an interval centred at zero, i.e. shifting in phase with heaving/pitching. Black corresponds to phase differences in an interval centred at π (out of phase) and two shades of grey correspond to intermediate phase differences.

A parcel of fluid moving along the fin at this value of V_x requires about two ($2\pi/3$ to be exact) flapping periods to travel the length of the fin, which is at the slow end of the range of oncoming flow speeds encountered by a typical tail fin in steady swimming. The four phase maps give the optimal phases of shifting relative to pitching and heaving, for maximizing output power and efficiency. As B and G vary, we find a sequence of bands of nearly constant phase. The transitions between the bands lie near values of (B, G) at which damped resonances occur, as explained (for B alone) in Alben (2008). Moving leftward in the phase maps, from one resonance to the next, the number of wavelengths present on the fin ray increases by approximately one half. The locations of the resonances depend only on the parameters (B, G, V_x), and are insensitive to the type of driving: heaving, pitching or shifting. In other mechanical systems it is typical to fix the elastic properties of the system, and then vary the driving frequencies to locate resonant frequencies. Here we have instead fixed the driving frequency (or V_x, inversely proportional to it) and find values of the elastic parameters (B, G) at which resonances occur. When G drops below 1 (0 on the log scale shown), the locations of the resonances become nearly independent of G, because the stiffness of the fin ray is provided mainly by B in this limit. At larger G, the resonances occur along oblique lines, because increasing G while decreasing B can result in a fin ray of approximately the same overall stiffness. Between the resonances, the optimal phases are nearly constant. For very stiff fin rays (right ends of the phase maps), shifting in phase with pitching or heaving yields the most output power. In contrast, shifting 180° out of phase yields the highest efficiency. These results recall those in Alben (2009*c*), where similar optimal phase differences between heaving and pitching were found for rigid foils. For more flexible foils, the optimal phases in figure 2 undergo a sequence of discrete jumps at each resonance.

In figure 3, we show the same quantities for an oncoming flow speed which is three times faster, $V_x = \pi$. For the stiffest foils (on the right-hand sides of the maps), the phases are relatively unchanged. For more flexible foils, there are notable differences. The spacings between the resonances are now decreased. Also, the jumps at the resonances are somewhat smaller than in figure 2, and there is somewhat more variation in phase between the resonances. There is a significant amount of variation

https://doi.org/10.1017/jfm.2011.506 Published online by Cambridge University Press

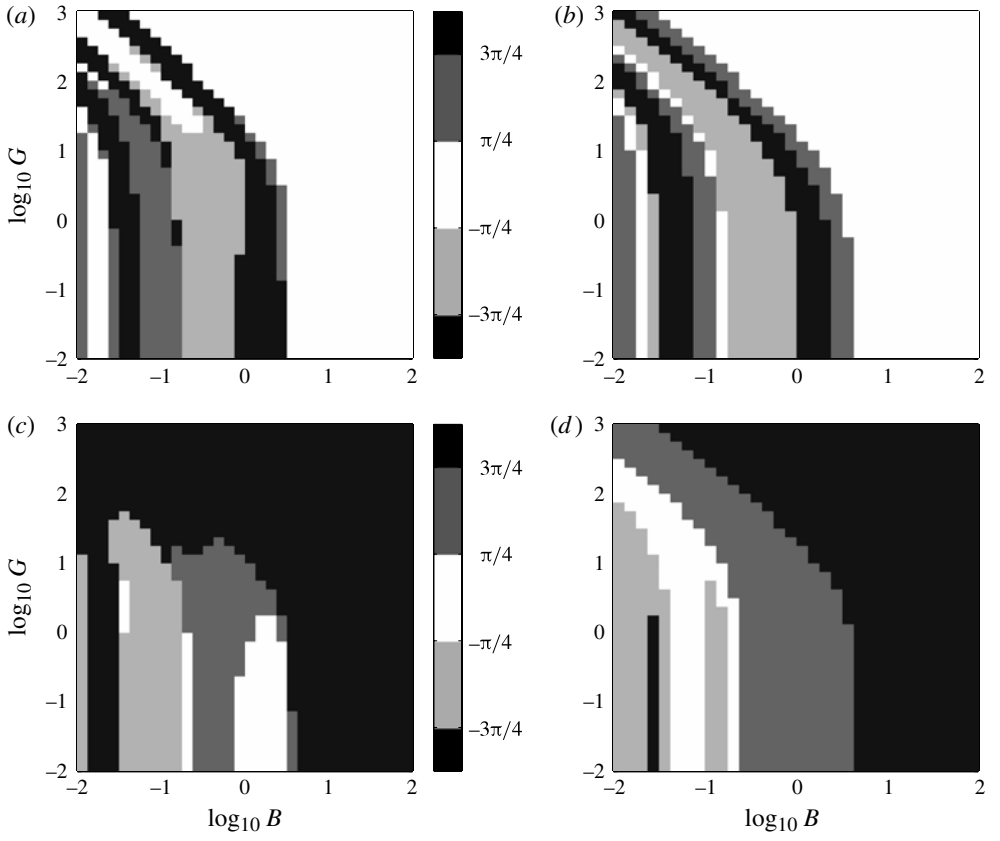


FIGURE 2. Greyscale maps of the optimal phases of shifting relative to heaving and pitching for maximizing output power and efficiency at dimensionless flow speed $V_x = \pi/3$. The values on the greyscale bar indicate the phase shifts, in radians, by which shifting should lead heaving or pitching, in order to optimize certain performance measures. The quantities plotted, one per panel, are given by (2.33), (2.34), (2.39) and (2.40). White indicates shifting nearly in phase with heaving/pitching, black indicates shifting nearly out of phase with heaving/pitching and grey indicates intermediate phase differences: (*a*) output-power maximizing phases for shifting relative to pitching (2.34), P_{out}, shift–pitch Δ phase; (*b*) output-power maximizing phases for shifting relative to heaving (2.33), P_{out}, shift–heave Δ phase; (*c*) efficiency maximizing phases for shifting relative to pitching (2.40), $P_{out} - P_{in}$, shift–pitch Δ phase; (*d*) efficiency maximizing phases for shifting relative to heaving (2.39), $P_{out} - P_{in}$, shift–heave Δ phase.

in the optimal phases for the most flexible foils (at the left sides of the maps), but generally, shifting should lead pitching/heaving temporally to maximize output power.

In appendix B we compare the magnitudes of the terms whose phases are given in (2.33), (2.34), (2.39) and (2.40) and figures 2 and 3. We find that the magnitudes are very similar for shifting with heaving versus shifting with pitching.

To obtain a more concrete picture of the results, we now give specific examples of the motions corresponding to the optimal shifting phases. In figure 4, we choose intermediate values of B and G, near unity, which correspond to moderately flexible fins: fins which exhibit bending modes similar to those observed in real tail fins. The value of V_x is $\pi/3$, the same as in figure 2. The values of B, G and V_x correspond

https://doi.org/10.1017/jfm.2011.506 Published online by Cambridge University Press

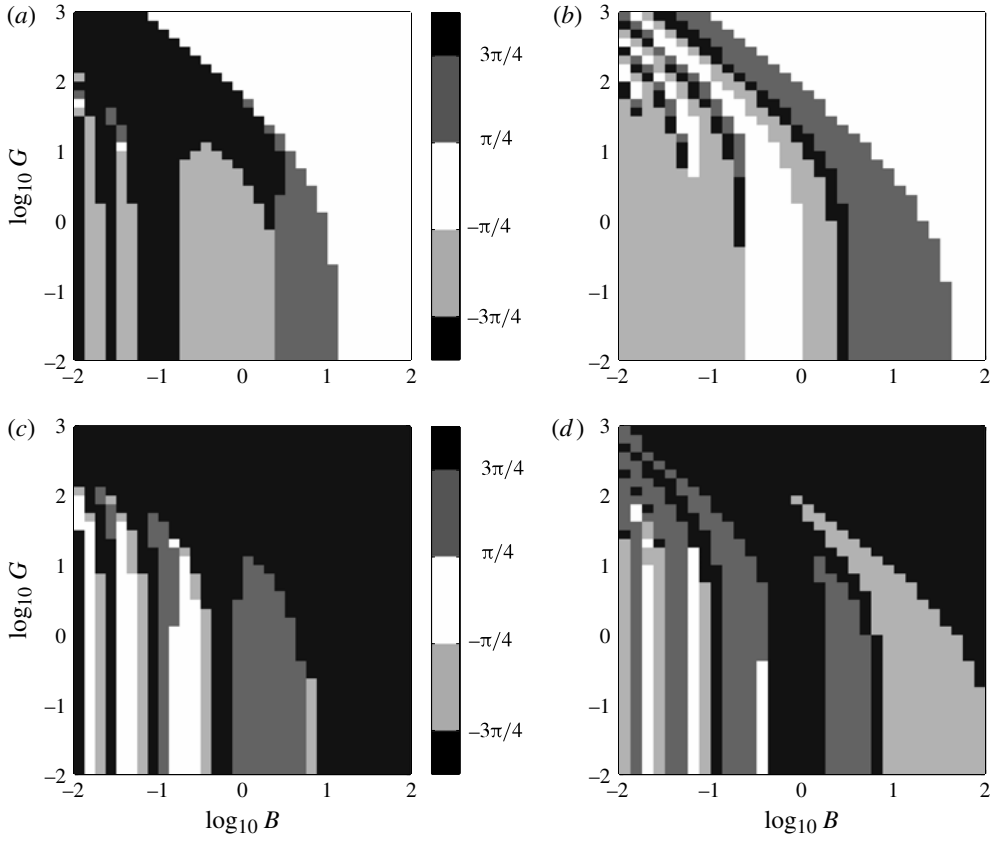


FIGURE 3. Same results as in figure 2 but now V_x is increased to π. The values on the greyscale bar indicate the phase shifts, in radians, by which shifting should lead heaving or pitching, in order to optimize certain performance measures. The quantities plotted, one per panel, are given by (2.33), (2.34), (2.39) and (2.40). White indicates shifting nearly in phase with heaving/pitching, black indicates shifting nearly out of phase with heaving/pitching, and grey indicates intermediate phase differences: (*a*) output-power maximizing phases for shifting relative to pitching (2.34), P_{out}, shift–pitch Δ phase; (*b*) output-power maximizing phases for shifting relative to heaving (2.33), P_{out}, shift–heave Δ phase; (*c*) efficiency maximizing phases for shifting relative to pitching (2.40), $P_{out} - P_{in}$, shift–pitch Δ phase; (*d*) efficiency maximizing phases for shifting relative to heaving (2.39), $P_{out} - P_{in}$, shift–heave Δ phase.

to the centres of the phase maps in figure 2. The top row shows 20 snapshots over a period for pure pitching and heaving motions, with arbitrary amplitudes. The next two rows show how the motions are modified when shifting at the optimal phases for maximizing output power (middle row) and efficiency (bottom row) are added. The amplitudes of the shifting motions are chosen to be comparable to those of the pitching and heaving motions. We make two basic observations. First, the motions which maximize P_{out} (middle row) have large amplitudes at the trailing edge. By contrast, the motions which maximize efficiency (bottom row) have smaller amplitudes at the trailing edge, which nearly equal those at the neighbouring maxima in the deflection envelopes. Large deflection at the trailing edge corresponds closely with the emission of large amounts of vorticity and kinetic energy into the wake. The

https://doi.org/10.1017/jfm.2011.506 Published online by Cambridge University Press

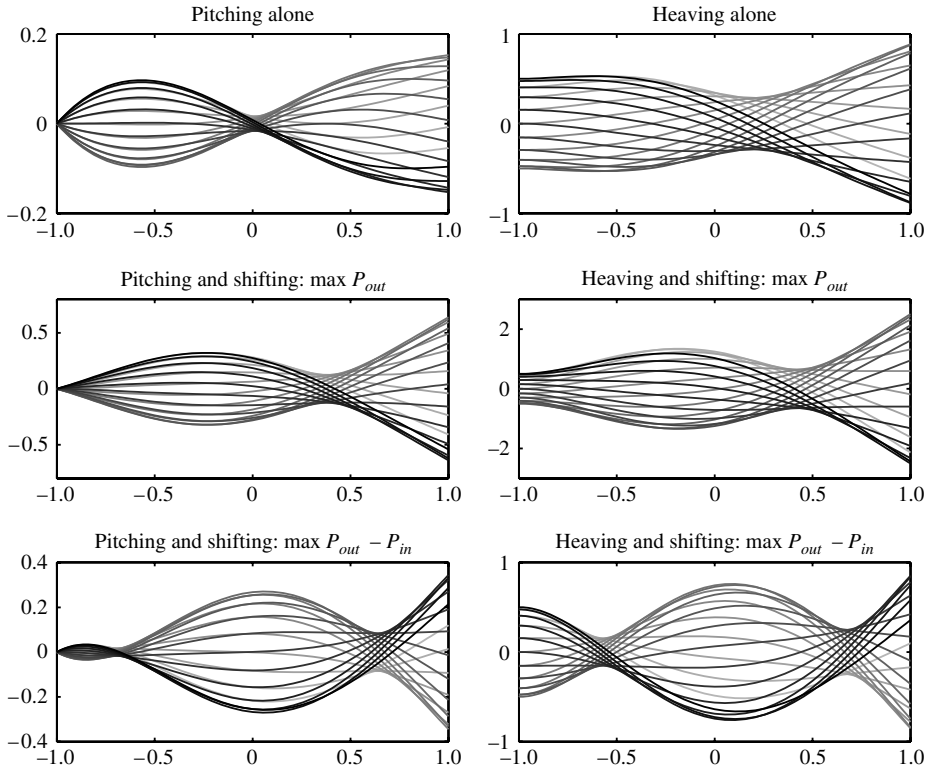


FIGURE 4. Examples of shifting motions superposed on pitching and bending motions, at the phases which maximize output power P_{out} and efficiency $P_{out} - P_{in}$. Here $B = 1$, $G = \sqrt{10}$ and $V_x = \pi/3$. Shades of grey increase from light to dark as the fin positions cycle through a period.

second observation is that the pure pitching and heaving motions (top row) look rather different from each other. By contrast, when optimal shifting is added, the combined motions become very similar, which can be seen by comparing shapes across columns in the middle and bottom rows. The main difference occurs at the leading edge, but this is unavoidable: the motions with heaving have non-zero amplitude at the leading edge, while those with pitching do not. Nonetheless, the motions look quite similar once one moves about one quarter length downstream.

We perform the same comparison of motions in figure 5, but now V_x is increased to π. Therefore, we are now considering motions at the points at the centres of the phase maps in figure 3. The resulting motions are somewhat less 'wavy' than in figure 2, but the same basic observations are true again. The motions which maximize power output have the largest trailing edge amplitude, while those which maximize efficiency have smaller trailing edge amplitude and a comparable peak in amplitude upstream. Also, the addition of optimal shifting leads to a convergence of the heaving and pitching motions (middle and bottom rows), although the starting points (top row) are more similar now than in figure 2.

We have given a linearized theory which calculates the shifting motions that maximize output power and efficiency for an oscillating flexible foil. One may ask: by how much do the optimal shifting motions increase these quantities? The answer

https://doi.org/10.1017/jfm.2011.506 Published online by Cambridge University Press

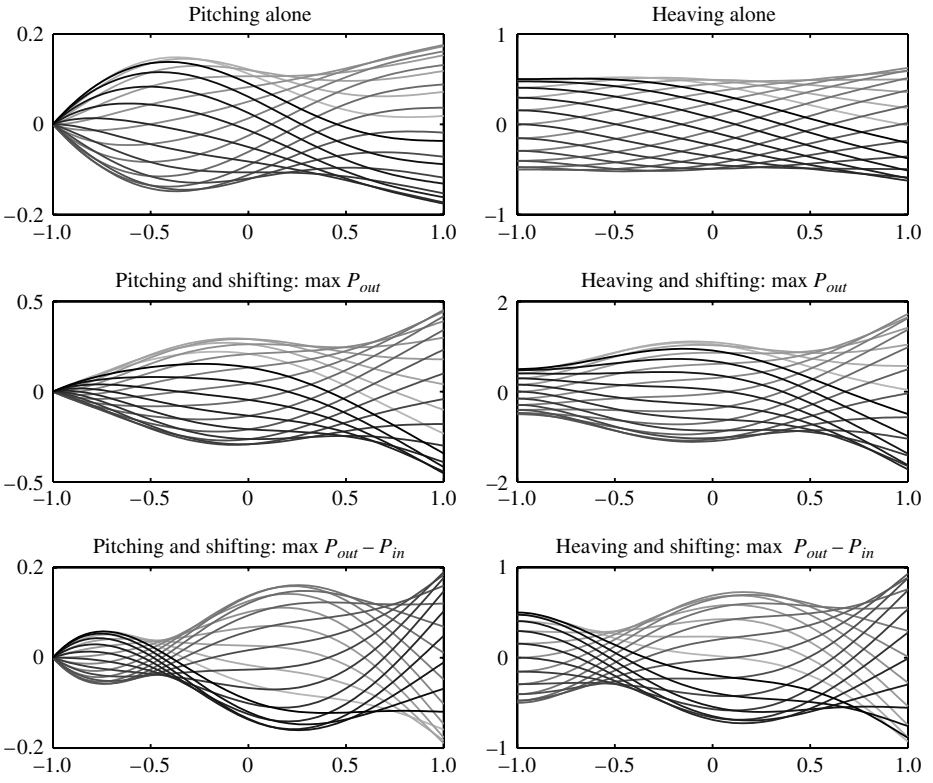


FIGURE 5. Same results as in figure 4 but now V_x is increased to π. Examples of shifting motions superposed on pitching and bending motions, at the phases which maximize output power P_{out} and efficiency $P_{out} - P_{in}$. Here $B = 1$, $G = \sqrt{10}$ and $V_x = \pi$. Shades of grey increase from light to dark as the fin positions cycle through a period.

is: it depends on the amplitudes of the driving motions, which are thus far unspecified. However, we now explain that optimal-phase shifting provides an $O(1)$ improvement in these quantities over pitching and heaving alone, when the amplitude of shifting approaches those of pitching and heaving. We first note that the magnitudes of the three 'pure' solutions corresponding to (2.20), (2.22) and (2.24) are all comparable: $O(1)$. Furthermore, as $|C_0| \nearrow |A_0|, |B_0|$, the contributions of the terms in the output power (2.29) which are proportional to A_0C_0, B_0C_0 (i.e. (2.32)) are comparable to the terms which are proportional to A_0^2, A_0B_0, B_0^2, which depend on heaving and pitching only. Thus, in general, the addition of shifting to a pure heaving or pure pitching motion, at the optimal relative phases, leads to an $O(1)$ increase in output power, at the limit of the regime where (2.30) holds. The same observation applies to input power, except now the optimal relative phase of shifting decreases P_{in} by $O(1)$. Thus, shifting generally leads to an $O(1)$ increase to the efficiency as well.

Acknowledgement

This work was supported by NSF-DMS grant numbers 0810602 and 1022619.

https://doi.org/10.1017/jfm.2011.506 Published online by Cambridge University Press

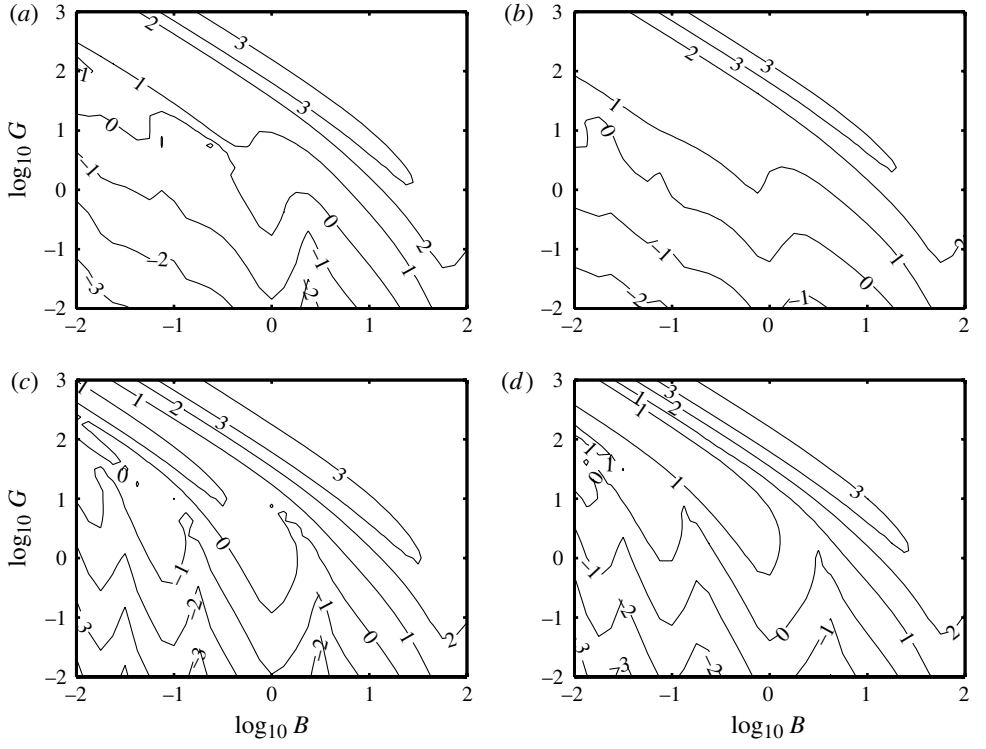


FIGURE 6. Contour plots showing the magnitudes of the power- and efficiency-maximizing contributions of the shifting–heaving and shifting–pitching motions to power and efficiency. These are the magnitudes of the terms whose arguments are given in (2.34) (*a*), (2.33) (*b*), (2.40) (*c*) and (2.39) (*d*). The contours are labelled by the logarithms, base 10, of the magnitudes. These are also the magnitudes corresponding to the phases given in figure 2. Here $V_x = \pi/3$: (*a*) P_{out}, shift–pitch magnitude; (*b*) P_{out}, shift–heave magnitude; (*c*) $P_{out} - P_{in}$, shift–pitch magnitude; (*d*) $P_{out} - P_{in}$, shift–heave magnitude.

Appendix A. Summary of inviscid flow model

We solve for the flow by posing a vortex sheet with strength $\gamma(x, t)$ on the fin and a vortex sheet wake with integrated strength (circulation) $\Gamma(x, t)$ set by the Kutta condition, which eliminates a velocity singularity at the vortex sheet shedding point, $x = 1$. The resulting equation for $[p]$ (explained in Alben 2008) is

$$[p] = \int_1^x \partial_t \gamma \, \mathrm{d}x' + V_x \gamma \tag{A 1}$$

where γ is set according to the condition that fluid does not penetrate the fin ray:

$$\frac{1}{2\pi} \int_{-1}^{1} \frac{\gamma(x', t) \, \mathrm{d}x'}{x - x'} = \partial_t y + V_x \partial_x y - \frac{1}{2\pi} \int_1^{\infty} \frac{\gamma(x', t) \, \mathrm{d}x'}{x - x'}. \tag{A 2}$$

With linear equations and boundary conditions (2.8) which are sinusoidal in time, the entire flow–fin-ray dynamics are periodic with a single frequency. In this case, the distribution of γ in the vortex sheet wake ($x > 1$) takes a particularly simple form. It is

https://doi.org/10.1017/jfm.2011.506 Published online by Cambridge University Press

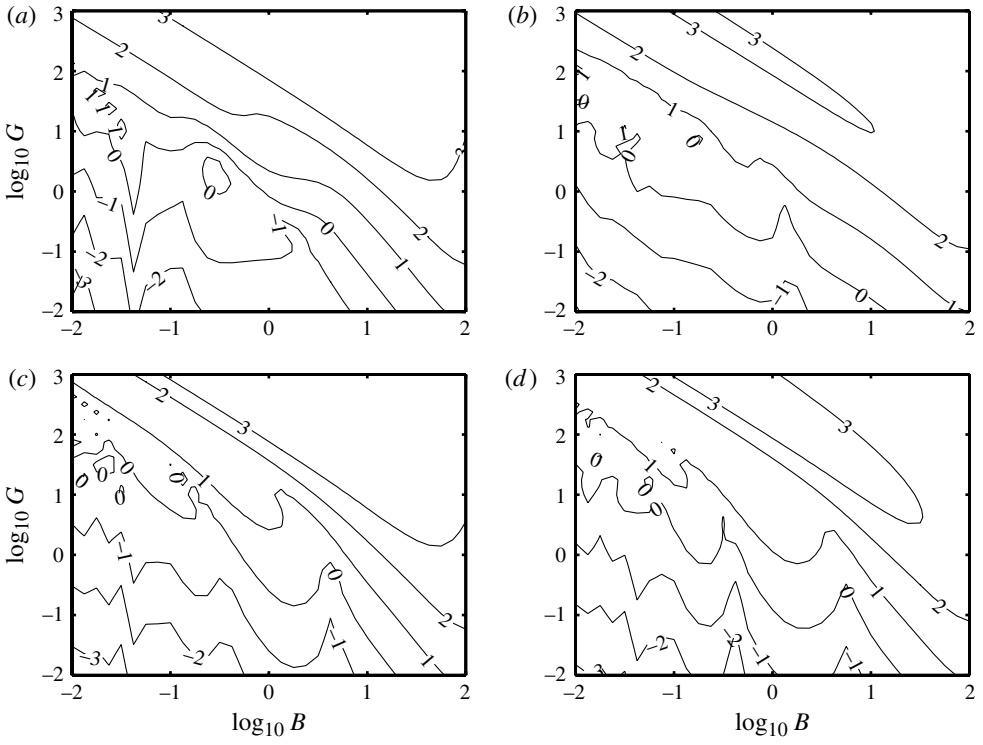


FIGURE 7. Contour plots showing the magnitudes of the power- and efficiency-maximizing contributions of the shifting–heaving and shifting–pitching motions to power and efficiency. These are the magnitudes of the terms whose arguments are given in (2.34) (*a*), (2.33) (*b*), (2.40) (*c*), and (2.39) (*d*). The contours are labelled by the logarithms, base 10, of the magnitudes. These are also the magnitudes corresponding to the phases given in figure 3. Here $V_x = \pi$: (*a*) P_{out}, shift–pitch magnitude; (*b*) P_{out}, shift–heave magnitude; (*c*) $P_{out} - P_{in}$, shift–pitch magnitude; (*d*) $P_{out} - P_{in}$, shift–heave magnitude.

convenient to express γ in terms of its integral, the circulation in the wake,

$$\Gamma(x,t) = \int_x^\infty \gamma(x',t)\,\mathrm{d}x'. \tag{A 3}$$

The circulation is conserved on parcels of fluid in the vortex sheet wake, which travel downstream with velocity V_x. Thus the circulation can be expressed in terms of the circulation at the trailing edge of the fin at an earlier time:

$$\Gamma(x,t) = \Gamma(1, t-(x-1)/V_x). \tag{A 4}$$

The circulation at the trailing edge of the fin varies sinusoidally in time:

$$\Gamma(1,t) = \mathrm{Re}\left(\Gamma_0 \mathrm{e}^{2\pi \mathrm{i} t}\right), \tag{A 5}$$

so the circulation and vorticity in the wake can be expressed in terms of the complex constant Γ_0 and a dimensionless frequency parameter $\Omega = 2\pi/V_x$:

$$\Gamma(x,t) = \mathrm{Re}\left(\Gamma_0 \mathrm{e}^{-\mathrm{i}\Omega(x-1)}\mathrm{e}^{2\pi \mathrm{i} t}\right) \tag{A 6}$$

$$\gamma(x,t) = \partial_x \Gamma(x,t) = \mathrm{Re}\left(-\mathrm{i}\Omega\Gamma_0 \mathrm{e}^{-\mathrm{i}\Omega(x-1)}\mathrm{e}^{2\pi \mathrm{i} t}\right). \tag{A 7}$$

https://doi.org/10.1017/jfm.2011.506 Published online by Cambridge University Press

Γ_0 is determined using the Kutta condition. The distribution of γ in $[-1, 1]$ which satisfies (A 2) can be written

$$\gamma(x, t) = \frac{v(x, t)}{\sqrt{1 - x^2}}, \tag{A 8}$$

where v is a bounded function. Thus γ has inverse square-root singularities. The Kutta condition sets $v(1, t) = \mathrm{Re}\left(V_1 e^{2\pi i t}\right)$ to zero. Setting the real and imaginary parts of V_1 to zero gives two equations which can be solved for two unknowns, the real and imaginary parts of Γ_0. The resulting explicit expression for Γ_0 is given in Alben (2008) and in an alternative, desingularized form in Alben (2009*b*).

Appendix B. Magnitudes of shifting contributions

In figures 6 and 7 we compare the magnitudes of the terms whose arguments are given in (2.33), (2.34), (2.39) and (2.40) and figures 2 and 3. We find that the magnitudes are very similar for the combinations of shifting with heaving and shifting with pitching. The reason is that heaving and pitching lead to shapes which are qualitatively similar at the same values of B and G. Thus the terms which are summed in (2.33), (2.34), (2.40) and (2.39) are of similar orders of magnitude. At smaller values of B and G, the Y and P terms are approximately sinusoidal and characterized by smaller wavelengths. The integrals in these equations scale inversely with the wavelengths of the (approximately sinusoidal) integrands. Thus the magnitudes of the shifting contributions plotted in figures 6 and 7 decrease with decreasing B and G.

REFERENCES

AKHTAR, I., MITTAL, R., LAUDER, G. V. & DRUCKER, E. 2007 Hydrodynamics of a biologically inspired tandem flapping foil configuration. *Theor. Comput. Fluid Dyn.* **21** (3), 155–170.

ALBEN, S. 2008 Optimal flexibility of a flapping appendage at high Reynolds number. *J. Fluid Mech.* **614**, 355–380.

ALBEN, S. 2009*a* On the swimming of a flexible body in a vortex street. *J. Fluid Mech.* **635**, 27–45.

ALBEN, S. 2009*b* Passive and active bodies in vortex–street wakes. *J. Fluid Mech.* **642**, 95–125.

ALBEN, S. 2009*c* Simulating the dynamics of flexible bodies and vortex sheets. *J. Comput. Phys.* **228** (7), 2587–2603.

ALBEN, S., MADDEN, P. G. & LAUDER, G. V. 2007 The mechanics of active fin-shape control in ray-finned fishes. *J. Roy. Soc. Interface* **4** (13), 243–256.

ALBEN, S. & MCGEE, R. L. 2010 Optimizing a fin ray for stiffness. *J. Mech. Phys. Solids* **58** (5), 656–664.

ALBEN, S., WITT, C., BAKER, T. V., ANDERSON, E. & LAUDER, G. V. 2011 Dynamics of freely swimming flexible foils. *Phys. Fluids* (submitted).

CHENG, J.-Y., PEDLEY, T. J. & ALTRINGHAM, J. D. 1998 A continuous dynamic beam model for swimming fish. *Phil. Trans. R. Soc. Lond.* B **353**, 981–997.

ELDREDGE, J. D., TOOMEY, J. & MEDINA, A. 2010 On the roles of chord-wise flexibility in a flapping wing with hovering kinematics. *J. Fluid Mech.* **659**, 94–115.

KATZ, J. & WEIHS, D. 1978 Hydrodynamic propulsion by large amplitude oscillation of an aerofoil with chordwise flexibility. *J. Fluid Mech.* **88** (3), 485–497.

LAUDER, G. V. 1989 Caudal fin locomotion in ray-finned fishes: historical and functional analyses. *Am. Zool.* **29** (1), 85.

LAUDER, G. V., ANDERSON, E. J., TANGORRA, J. & MADDEN, P. G. 2007 Fish biorobotics: kinematics and hydrodynamics of self-propulsion. *J. Expl Biol.* **210** (Pt 16), 2767.

LAUDER, G. V. & MADDEN, P. G. A. 2007 Fish locomotion: kinematics and hydrodynamics of flexible foil-like fins. *Exp. Fluids* **43** (5), 641–653.

https://doi.org/10.1017/jfm.2011.506 Published online by Cambridge University Press

LIGHTHILL, MJ 1970 Aquatic animal propulsion of high hydromechanical efficiency. *J. Fluid Mech.* **44** (02), 265–301.

MICHELIN, S. & SMITH, S. G. L. 2009 Resonance and propulsion performance of a heaving flexible wing. *Phys. Fluids* **21**, 071902.

MILLER, L. A. & PESKIN, C. S. 2009 Flexible clap and fling in tiny insect flight. *J. Expl Biol.* **212** (19), 3076.

MITTAL, R. 2004 Computational modelling in biohydrodynamics: trends, challenges, and recent advances. *IEEE J. Ocean. Engng* **29** (3), 595–604.

PAIDOUSSIS, M. P. 1998 *Fluid–Structure Interactions, Vol 2: Slender Structures and Axial Flow*. Academic Press Inc.

PEDLEY, T. J. & HILL, S. J. 1999 Large-amplitude undulatory fish swimming: fluid mechanics coupled to internal mechanics. *J. Expl Biol.* **202**, 3431–3438.

PREMPRANEERACH, P., HOVER, F. S. & TRIANTAFYLLOU, M. S. 2003 The effect of chordwise flexibility on the thrust and efficiency of a flapping foil. In *International Symposium on Unmanned Untethered Submersible Technology*, University of New Hampshire, Durham, NH.

SCHULTZ, W. *et al*. 2002 Power requirements of swimming: do new methods resolve old questions? *Integr. Compar. Biol.* **42** (5), 1018.

SHELLEY, M. J. & ZHANG, J. 2011 Flapping and bending bodies interacting with fluid flows. *Annu. Rev. Fluid Mech.* **43**, 449–465.

TANGORRA, J., ANQUETIL, P., FOFONOFF, T., CHEN, A., DEL ZIO, M. & HUNTER, I. 2007 The application of conducting polymers to a biorobotic fin propulsor. *Bioinspir. Biomimet.* **2**, S6.

VIDELER, J. J. 1993 *Fish Swimming*. Springer.

WANG, Z. J. 2005 Dissecting insect flight. *Annu. Rev. Fluid Mech.* **37**, 183–210.

WU, T. 1971 Hydromechanics of swimming propulsion. Part 2. Some optimum shape problems. *J. Fluid Mech.* **46** (03), 521–544.

ZHU, Q. & SHOELE, K. 2008 Propulsion performance of a skeleton-strengthened fin. *J. Expl Biol.* **211** (Pt 13), 2087.

https://doi.org/10.1017/jfm.2011.506 Published online by Cambridge University Press